Measurements of Energy Transport Patterns in Solid Density Laser Plasma Interactions at Intensities of 5×10^{20} W cm^{-2}

K. L. Lancaster,[1] J. S. Green,[1,2] D. S. Hey,[3,4] K. U. Akli,[3,4] J. R. Davies,[5] R. J. Clarke,[1] R. R. Freeman,[6] H. Habara,[7] M. H. Key,[4] R. Kodama,[7,8] K. Krushelnick,[2] C. D. Murphy,[1,2] M. Nakatsutsumi,[7] P. Simpson,[9] R. Stephens,[10] C. Stoeckl,[11] T. Yabuuchi,[7] M. Zepf,[9] and P. A. Norreys[1,2]

[1]*CCLRC, Rutherford Appleton Laboratory, Chilton, Oxon, OX11 0QX, United Kingdom*
[2]*Blackett Laboratory, Imperial College London, Prince Consort Road, London SW7 2BZ, United Kingdom*
[3]*Department of Applied Sciences, University of California, 1 Shields Avenue, Davis, California 95616-8254, USA*
[4]*Lawrence Livermore National Laboratory, P.O. Box 808, Livermore, California 94550, USA*
[5]*GoLP/Centro de Fisica dos Plasmas, Instituto Superior Técnico, 1049-001 Lisbon, Portugal*
[6]*Department of Physics, Ohio State University, Columbus, Ohio 43210-1117, USA*
[7]*Graduate School of Engineering, Osaka University, Suita, 565-0871 Osaka, Japan*
[8]*Institute of Laser Engineering, Osaka University, Suita, 565-0871 Osaka, Japan*
[9]*Departments of Pure and Applied Physics, Queens University, Belfast BT7 1NN, United Kingdom*
[10]*General Atomics, P.O. Box 86508, San Diego, California 92186-5608, USA*
[11]*Laboratory of Laser Energetics, University of Rochester, 250 East River Road, Rochester, New York 14623, USA*

K_α x-ray emission, extreme ultraviolet emission, and plasma imaging techniques have been used to diagnose energy transport patterns in copper foils ranging in thickness from 5 to 75 μm for intensities up to 5×10^{20} W cm^{-2}. The K_α emission and shadowgrams both indicate a larger divergence angle than that reported in the literature at lower intensities [R. Stephens *et al.*, Phys. Rev. E **69**, 066414 (2004)]. Foils 5 μm thick show triple-humped plasma expansion patterns at the back and front surfaces. Hybrid code modeling shows that this can be attributed to an increase in the mean energy of the fast electrons emitted at large radii, which only have sufficient energy to form a plasma in such thin targets.

Knowledge of energy transport processes in overdense laser-plasma interactions is fundamental to the evaluation of the fast ignition concept [1] and the optimization of ion acceleration processes [2]. These interactions have been the subject of intensive investigation over the past few years. The first experiments using the VULCAN 10 TW laser facility indicated that the fast electron flow was collimated due to self-generated magnetic fields [3]. This was inferred from shadowgrams obtained by a transverse optical probe taken 200 ps after the interaction. They showed a plasma on the rear surface of thick plastic targets with a lateral size less than that of the laser focal spot [3].

Jetlike structures inside transparent glass targets were also observed using the same technique by another team, using somewhat higher laser powers [4]. Those measurements were taken a few picoseconds after the interaction pulse. Gremillet *et al.* [5] later observed similar jets, but this was followed by a slower moving hemispherical ionization front. They concluded that there was only a small amount of energy in the jets imaged in the shadowgrams.

Optical measurements from the rear surface of thin metal foil targets (attributed to optical transition and thermal emission radiation) were made at the LULI [6] and GEKKO XII [7] 100 TW facilities. The divergence of the flow patterns was inferred to be 34° and 20°–30°, respectively. Stephens *et al.* [8] measured energy transport patterns that indicated a divergence of 40° using metallic sandwich targets irradiated with the VULCAN and LULI

laser systems for intensities up to 5×10^{19} W cm^{-2}. The divergent flow was diagnosed using Cu K_α imaging of the rear surface with the Cu buried layer at different points in the target.

Annular transport patterns have been reported for low atomic number and low density targets irradiated with PW laser pulses. Koch *et al.* [9] observed annular transport patterns using x-ray pinhole imaging, and Jung *et al.* [10] observed a double ring structure using optical transition radiation imaging of the rear surface.

In this Letter, a comparison of the different measurement techniques was undertaken for the first time at intensities on target up to 5×10^{20} W cm^{-2}, an order of magnitude higher than any previous study at solid density. Shadowgraphy, thermal radiation from the rear surface using extreme ultraviolet (XUV) imaging, and Cu K_α x-ray imaging were deployed on the same shots to see if there are any systematic differences between them. This information is important, because previous work described above used different techniques to measure the energy transport, and each one is dependent on different variables. In general, it was found that the observed energy transport patterns were divergent. The beam divergence inferred from the K_α imaging is larger than that reported in the previous literature at lower intensities [8]. This suggests that the global magnetic field that acts to focus the beam may be reduced as the intensity on the target is raised, as predicted by the Davies rigid beam model [11].
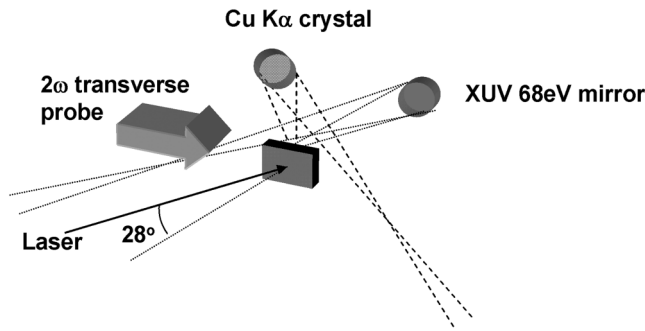
125002-1

FIG. 1. Experimental configuration inside the target chamber.

The experiments described in this Letter were conducted using the VULCAN petawatt laser facility [12]. The petawatt laser delivered up to 250 J of p-polarized, $\lambda = 1.05$ μm light onto a target contained in a pulse of duration $450(\pm 50)$ fs. The laser was focused onto the target using an $F/3$ off-axis parabolic mirror to a spot size of 7 μm diameter. Approximately 30% of the energy was contained within the central focal spot, giving peak intensities up to 5×10^{20} W cm^{-2}. The parametric fluorescence due to the optical parametric chirped pulse amplification was 5×10^{-8}, up to 2 nanoseconds ahead of the interaction pulse. Closer to the pulse, this level fluctuated between 10^{-6} and 10^{-8} on a shot by shot basis. This was superimposed on the amplified spontaneous emission background of 10^{-9} extending to 10 ns ahead of the pulse. The main pulse, therefore, is interacting with preformed plasma. The laser was incident onto the target at an angle of 28°. The targets were 2 mm $\times$ 4 mm Cu foils of thickness 5–75 μm to diagnose electron transport using K_α and XUV rear surface imaging. Transverse probing was used to image the global plasma expansion from the front and the rear of thin Cu targets. Figure 1 shows a schematic of the experimental layout.

The Cu K_α radiation (8.05 keV) emitted from the target was focused using a spherically curved quartz 211 crystal onto a Princeton Instruments 16 bit CCD camera [13]. This produced an image of the back surface of a Cu target. The magnification of the system was 17.4, with a spatial reso-

lution $\sim$20 μm. The XUV radiation emitted at 68 eV from the heated region on the rear surface was imaged using a spherical multilayer mirror onto a Princeton Instruments 16 bit CCD camera. This produced an image of the emission region at the rear surface of the target. The magnification was 12, and the spatial resolution was 10 μm. The spectral bandwidth (10 eV) was determined by the mirror and filters (1 μm Al, 0.15 μm polypropylene), and, since the system is temporally integrated, a component of the emission observed will be from recombinant processes as the plasma cools.

The expansion on the front and back surfaces of the target were diagnosed using a transverse optical probe. A small part of the main PW beam was diverted into the probe system. The 1.054 μm light was frequency doubled to 527 nm using a potassium dihydrogen phosphate crystal. The duration of the probe beam was the same duration as the main beam. An optical streak camera was used to synchronize the probe beam to the main beam. Images were taken at 200 ps after the interaction, at which point the expansion on the front and back surfaces was observed for most target thicknesses. The shadowgraphy images were recorded using an 8 bit CCD camera connected to a personal computer via image acquisition software. The resolution of the probe system was found to be $\sim$12 μm, the magnification was 4, and the f number was 12. Images produced by this technique show dark regions where the density exceeds roughly 10^{19} cm^{-3}, due to the large density gradients. The variation in the density gradient with prepulse intensity makes it difficult to estimate the lowest density in the obscured region. Previous work indicates a limit of around 5×10^{19}–1×10^{20} cm^{-3} [14].

Figure 2 shows shadowgrams taken at a time 200 ps after the interaction. Figures 2(a)–2(c) are Cu targets of thickness 25, 50, and 75 μm, respectively. The expansion at the back surface shows that this region has been heated. The spatial extent of the inaccessible region (on the laser axis) to the baseline expansion along the rest of the target surface was measured. The full width at half maximum (FWHM) was then calculated to obtain the spot size. Figure 2 shows that these features increase in size with
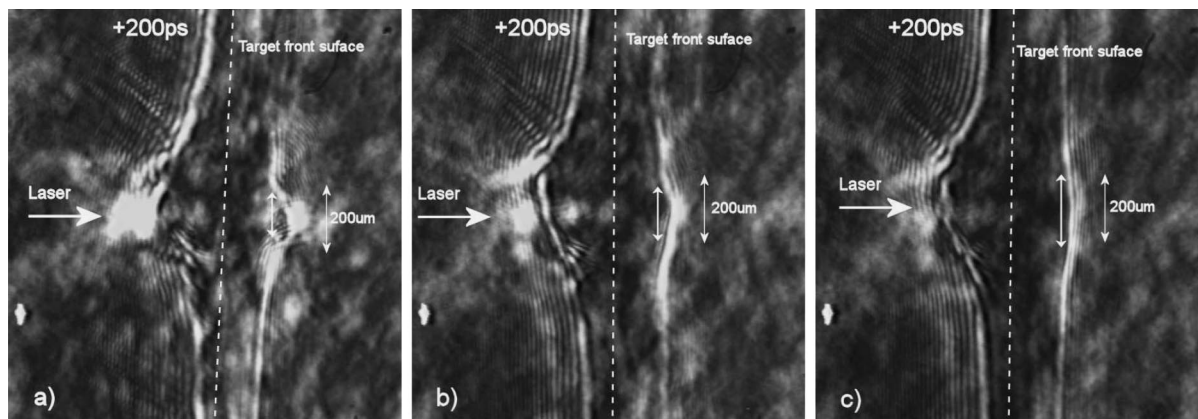
FIG. 2. Shadowgrams of Cu foils of thickness (a) 25, (b) 50, and (c) 75 μm.

target thickness. This indicates that the heated region at the back surface is divergent.

The size of the Cu K_α emission region was also measured on the same shots. The spot sizes were obtained from measuring the FWHM of the Cu K_α image and correcting for view angle foreshortening. The radii of the spot sizes derived from Cu K_α and shadowgraphy images were plotted against position as shown in Fig. 3. The radii were plotted to allow the divergence angle to be calculated from the gradient using $2 \times \arctan(m)$, where m is the gradient. The depth in the Cu K_α case is a transmission weighted average which is defined as $\int_0^L x \exp(-x/\alpha) / \int_0^L \exp(-x/\alpha)$, where x is the position, α is the attenuation length of Cu K_α in solid Cu, and L is the target thickness. The straight line was fitted to the data using a least squares technique. The error bars are calculated from the shot to shot fluctuation. The full cone angle divergence was calculated to be 76° and 54° for the shadowgraphy and K_α, respectively. The divergences differ between techniques, as the K_α depends on the energy density of electrons above the line energy but the shadowgraphy is measuring plasma expansion, which depends on the electron temperature. It interesting to note that the K_α divergence angle is larger than that reported in previous literature for lower intensities on target. This is consistent with the Davies rigid beam model, where the focusing magnetic field is reduced as the temperature rises after the Spitzer regime is entered [11]. On the other hand, one cannot rule out the cone angle that the electrons are generated with may increase with intensity. This requires further experimental investigation.

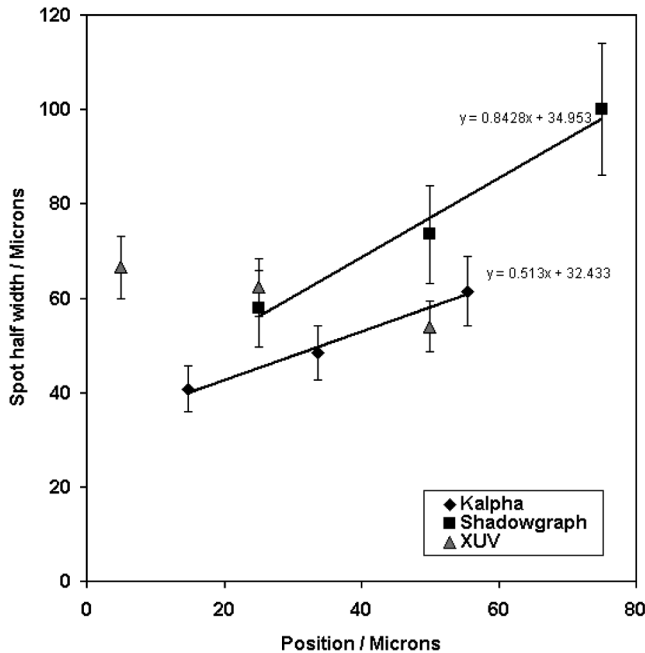At a target thickness of 5 μm, unusual features were visible at the front and back surfaces of the target using

shadowgraphy. Figure 4 shows an image of a 5 μm Cu target taken at a time 200 ps after the interaction. On the back surface there is a "triple-humped" feature that is reproduced with a larger spatial scale on the front surface. The back surface feature resembles an annular beam surrounding a central collimated region. This pattern was observed only in the thinnest targets.

A similar triple-humped feature has been observed on the back of 175 μm thick Mylar targets in previous experiments on the VULCAN 100 TW system, as reported by Norreys *et al.* [15], where an extensive discussion of possible causes is given. They concluded that the beam hollowing mechanism described by Davies [11,16] was the most likely explanation, which is caused by the concentration of the return current on the beam axis due to the lower resistivity caused by Ohmic heating.

To investigate this in more detail, we used the hybrid code, as described in Refs. [11,16]. In the work presented here, it was found that the mean energy of the fast electrons reflected from the back surface was closely correlated to the shape of the plasma observed in the experiments, as would be expected since plasma expansion velocity is determined by the electron temperature. Mean energy was used in place of temperature (kT) since this is a more clearly defined quantity, although it varies from $kT/2$ for a one-dimensional Maxwellian with $kT \ll mc^2$ to $3kT$ for a three-dimensional Maxwellian with $kT \gg mc^2$, and the energy distribution obtained in the code was not precisely Maxwellian. Therefore, in Fig. 5, the mean kinetic energy of the fast electrons striking the back surface of a 5 μm thick Cu target is given. The shape of the curves correlates well with the shape of the plasma observed, having a central peak and broad wings. The rise in the mean energy in these wings is not, however, due to beam hollowing, which leads to the small peaks just off axis. It is due to the collisional, energy filtering effect of the target removing lower energy electrons, an effect that is always present but which has never been of particular interest
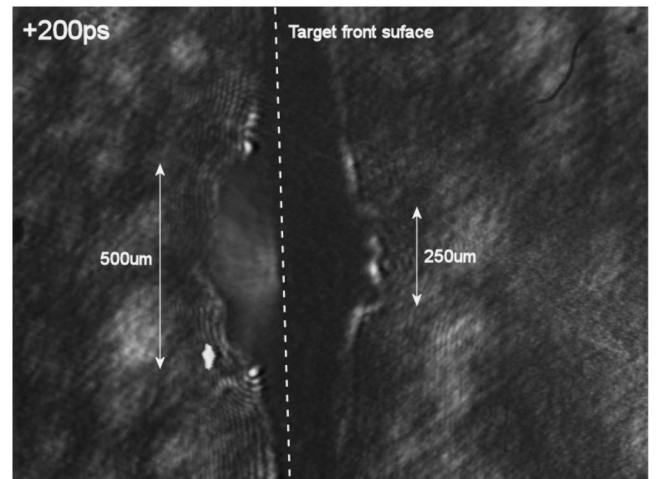

FIG. 3. Plot of K_α, shadowgraphy, and XUV radii vs position.

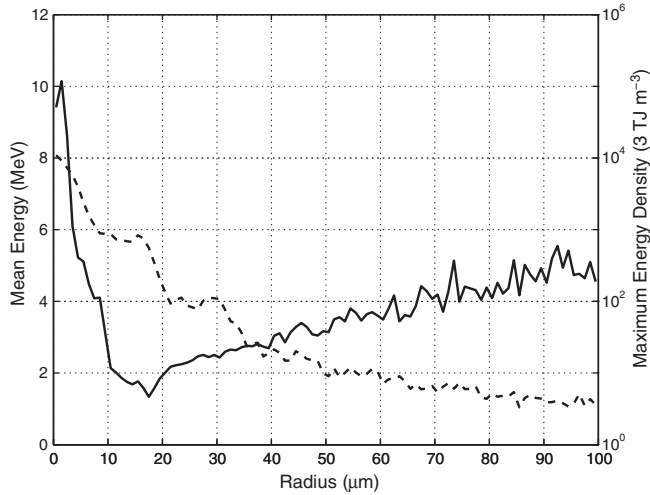FIG. 4. Shadowgram of a 5 μm thick Cu target taken at +200 ps with respect to the main pulse.

FIG. 5.   Mean energy of the fast electrons striking the back surface of a 5 μm thick Cu target (solid line) and maximum energy density of fast electrons in units of 3 TJ m^{-3} (dotted line) given by the hybrid code. A 1 μm bin width was used, twice the grid spacing.

since it involves a very small fraction of the electron energy. The sheath electric field that would be generated by the electrons at the target surface, before any ion motion occurs, will exceed the field ionization threshold of 0.5 TV m^{-1} when the energy density is greater than roughly 3 TJ m^{-3}. The energy density also presented in Fig. 5 shows that this threshold is reached at radii as large as 90 μm, and this suggests that a plasma would be rapidly formed on the target surfaces up to this radius, so the ''wings'' would be expected to be visible, a result of the high intensity and small target thickness. According to these criteria, these wings would not be visible in the thicker targets. This work suggests that the cause of this annular pattern is not likely to be beam hollowing.

The structure was not observed with the other imaging techniques. This is consistent with the shape of the plasma being determined by the mean energy of the fast electrons, because the other diagnostics are expected to be determined by different parameters as stated previously.

The XUV spot sizes were also derived from the FWHM of the signal strength in an identical way to the Cu K_α and are shown in Fig. 3. The XUV of the depth is simply the target thickness (the optical depth of 68 eV photons in Cu is 1–2 μm, so it is safe to assume the biggest signal is from the rear surface of the target). The temperature at the back surface is expected to fall with increasing target thickness, since the energy reaching the back surface is reduced, and this almost certainly accounts for the observed reduction in the size of the heated region. Indeed, the decrease in spot size observed in the XUV data with the target thickness in Fig. 3 is reproduced using the hybrid code, albeit with a much smaller FWHM (due to the absence of thermal

conduction and hydrodynamic expansion in the calculations). The K_α spot size inferred from the hybrid code was found to be strongly dependent on the fast electron refluxing. Total refluxing (specular reflection of particles from the front and back) gave a spot size that tended to decrease with increasing target thickness. Partial refluxing (specular reflection at the back, removal at the front) gave a spot size that increased with target thickness but which was too small for the thinner targets. Further work on this and on relating the hybrid code results to the experimental diagnostics is required.

In summary, the first comparison of different imaging techniques was performed (shadowgraphy, thermal radiation from the rear surface using XUV imaging, and Cu K_α imaging) on the same shots for petawatt laser-plasma interactions. The observed energy transport patterns were divergent. The K_α beam divergence of 54° is larger than the 40° divergence angle measured at lower intensities on target. In 5 μm thick Cu foils, an annular heated region surrounding a collimated region was revealed. Ultimately, this work confirms that, to diagnose energy transport across a broad range of electron energies, one must implement a range of imaging techniques.

[1] M. Tabak *et al.*, Phys. Plasmas **1**, 1626 (1994).
[2] E. L. Clark *et al.*, Phys. Rev. Lett. **84**, 670 (2000); R. A. Snavely *et al.*, Phys. Rev. Lett. **85**, 2945 (2000); E. L. Clark *et al.*, Phys. Rev. Lett. **85**, 1654 (2000).
[3] M. Tatarakis *et al.*, Phys. Rev. Lett. **81**, 999 (1998).
[4] M. Borghesi *et al.*, Phys. Rev. Lett. **83**, 4309 (1999).
[5] L. Gremillet *et al.*, Phys. Rev. Lett. **83**, 5015 (1999).
[6] J. J. Santos *et al.*, Phys. Rev. Lett. **89**, 025001 (2002).
[7] R. Kodama *et al.*, Nature (London) **412**, 798 (2001).
[8] R. Stephens *et al.*, Phys. Rev. E **69**, 066414 (2004).
[9] J. Koch *et al.*, Phys. Rev. E **65**, 016410 (2001).
[10] R. Jung *et al.*, Phys. Rev. Lett. **94**, 195001 (2005).
[11] J. R. Davies, Phys. Rev. E **68**, 056404 (2003).
[12] C. N. Danson *et al.*, Nucl. Fusion **44**, S239 (2004).
[13] J. A. King *et al.*, Appl. Phys. Lett. **86**, 191501 (2005).
[14] P. A. Norreys *et al.*, Phys. Plasmas **6**, 2150 (1999).
[15] P. A. Norreys *et al.*, Plasma Phys. Controlled Fusion **48**, L11 (2006).
[16] J. R. Davies *et al.*, Plasma Phys. Controlled Fusion (to be published).